Crossian Resonance

A Multidisciplinary Research Journal **ISSN 0976-5417**
(A refereed Biannual Published in June and December)
Vol. 15, No.2, December 2024
https://research.holycrossngl.edu.in/

Modified $CuO-Mn_2O_3$ and $CuO-Fe_2O_3$ Nanocomposites Synthesized Via Ultrasonication- Assisted Co-Precipitation for Sensor Applications

Lifna Serene R.J., Antony Arokya Sangeetha Devi A., Jenima J. and
***Priya Dharshini M.**
Department of Physics, Holy Cross College (Autonomous), Nagercoil - 629 004
Affiliated to Manonmaniam Sundaranar University, Tirunelveli - 627 012

ABSTRACT

Modified $CuO-Mn_2O_3$ and $CuO-Fe_2O_3$ nanocomposites were synthesized via ultrasonication-assisted co-precipitation method. The method combines the high reactivity of co-precipitation with sonication capability to produce homogeneously dispersed nanoparticles with enhanced surface properties. The structural characteristics of the nanocomposites were examined using X-ray diffraction (XRD), confirming the successful formation of $CuO-Mn_2O_3$ and $CuO-Fe_2O_3$ phases. UV-Vis spectroscopy and Photoluminescence (PL) analysis were used to investigate the optical properties of the synthesized nanocomposites, offering valuable information about their electronic structures and band gaps, which are essential for improving sensitivity in sensor applications.
Keywords: *Nanocomposites, Oxide, PXRD, Absorption*

1. Introduction

In recent years, nanoscale structures have garnered significant interest from the research community due to their remarkable physical, chemical, mechanical, and electrical properties. [1,2]. Nanocomposites are a fascinating application of nanoscience. They are materials composed of a matrix embedded with nanoparticles or nanostructures. The inclusion of these nanomaterials can greatly improve the properties of composite materials [3,4]. Copper oxide (CuO) nanostructures are particularly intriguing due to their unique properties and potential applications in batteries, supercapacitors, solar cells, gas sensors, biosensors, nanofluids, catalysis, photodetectors, energetic materials, field emission, superhydrophobic surfaces, and the removal of arsenic and organic pollutants from wastewater. When combined with Mn_2O_3 and Fe_2O_3, CuO-based nanocomposites can further enhance these properties [5-6].

2. Materials and Methods

In this project work, high quality $CuO-Mn_2O_3$ and $CuO-Fe_2O_3$ nanocomposites are synthesized by ultrasonication assisted co-precipitation method. Cupric sulphate (7.490 g)

***Corresponding Author:** priyadharshini@holycrossngl.edu.in*

was dissolved in 100 ml of distilled water and stirred for 60 minutes using a magnetic stirrer. Separately, manganese acetate (7.3527 g) was dissolved in 100 ml of distilled water and stirred thoroughly. Both the cupric sulphate and manganese acetate solutions were then combined. Next, Sodium hydroxide was dissolved in 100 ml of distilled water and stirred well. The sodium hydroxide solution was added drop by drop to the mixed solution while maintaining a pH of 10. The resulting precipitate was placed in an ultrasonicator (Powersonic 405S) and washed five times with double-distilled water, followed by two washes with ethanol and double-distilled water. The precipitate was then dried in a hot air oven at 100°C. The resulting sample was brown in color. After grinding, the sample was heated in a muffle furnace at 400°C for two hours, yielding a black CuO-Mn_2O_3 nanopowder. A similar procedure was followed for the synthesis of CuO-Fe_2O_3 nanocomposites, using cupric sulphate and ferric chloride as precursors.

3. Results and Discussion

PXRD analysis

The structural characterization of the CuO-Mn_2O_3 and CuO-Fe_2O_3 nanocomposites were analyzed by recording the powder X-ray diffraction (PXRD) spectra using an X-ray diffractometer. The crystal grain size can be quantitatively estimated using the Scherrer equation and the diffraction peak broadening in the XRD curves.

$$D = \frac{0.9\lambda}{\beta\cos\theta}$$

Where λ is the wavelength of the Cu- K_α radiation [1.54060 Å], β is the full width half maximum of the diffraction line and θ is the angle of diffraction. Figure 1 displays the PXRD pattern of the synthesized CuO-Mn_2O_3 nanocomposites, with peaks observed at (222), (431), (521), and (026) corresponding to 2θ values of 32.95°, 49.35°, 53.29°, and 62.37°, respectively. The CuO peaks are observed at (002), (111), (022), and (004), corresponding to 2θ values of 35.39°, 38.29°, 64.98°, and 75.01°, respectively. The Mn_2O_3 peak, corresponding to (002), exhibits a high relative intensity. The average grain size, D, is 21.39 nm. The 2θ values obtained from the PXRD data for Mn_2O_3 in the CuO-Mn_2O_3 nanocomposites closely match those of the JCPDS File No. 65-1798, and its structure is determined to be cubic. The CuO structure in the synthesized CuO-Mn_2O_3 nanocomposites is monoclinic. Figure 2 shows the PXRD pattern of the CuO-Fe_2O_3 nanocomposites. The peaks for Fe_2O_3 are observed at (011), (013), (201), (211), (114), (214), and (330) with 2θ values of 13.75°, 30.15°, 36.504°, 37.95°, 43.50°, 53.94°, and 63.23°, respectively. The CuO peaks are observed at (004) and (202), corresponding to 2θ values of 58.16° and 75.01°. The CuO peak at (201) exhibits the highest relative intensity. The 2θ values for iron oxide in the

CuO-Fe_2O_3 nanocomposites match well with the JCPDS File No. 89-7047, and the structure is determined to be orthorhombic. The structure of CuO was monoclinic in the synthesized CuO-Fe_2O_3 nanocomposites. The average grain size D is 20.554389 nm [7].

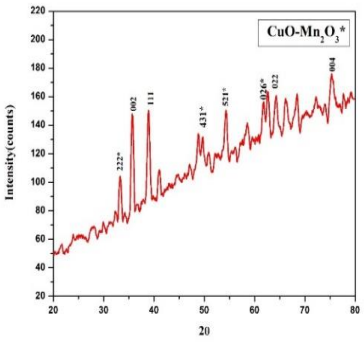

Fig. 1. PXRD pattern of CuO – Mn_2O_3 Nanocomposites

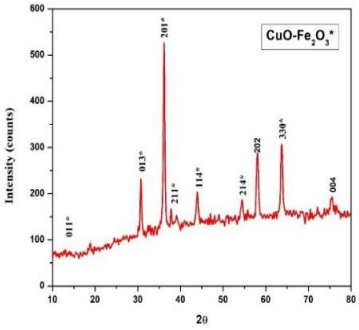

Fig. 2. PXRD pattern of CuO-Fe_2O_3 Nanocomposites

Photoluminescence (PL) analysis

Photoluminescence (PL) studies for the synthesized CuO- $Mn_2O_3$and CuO- Fe_2O_3 nanocomposites were carried out using a photoluminescence spectrophotometer and the emission spectra were recorded at a scan rate of 600 nm/min using the excitation wavelength of 320 nm. The PL emission spectra of CuO-Mn_2O_3 and CuO- Fe_2O_3 nanocomposites exhibit a prominent peak at 358 nm, which corresponds to blue emission, likely due to the radiative recombination of charge carriers or defect states involving Mn^{2+} or Mn^{3+} ions. The smaller peaks at 388 nm and 406 nm are attributed to blue-green emissions, which are associated with defect states or surface defects, possibly linked to oxygen vacancies in the material. The peak at 489 nm corresponds to green emission, likely arising from electron-hole recombination or shallow defects, while the 570 nm peak is a yellow emission, which is typically related to deep-level trap states or significant defects, such as oxygen vacancies. For the CuO-Fe_2O_3 nanocomposites, the primary peak at 358 nm also corresponds to blue emission, and the smaller peaks at 387 nm and 406 nm indicate blue-green emissions due to similar defect-related phenomena involving oxygen vacancies or point defects in the CuO-Fe_2O_3 matrix [8].

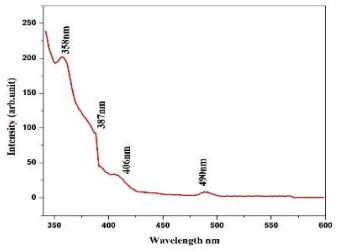

Fig. 3. PL spectra of CuO- Mn_2O_3 Nanocomposites

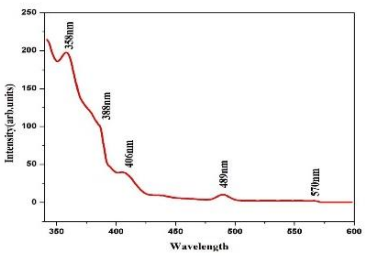

Fig. 4. PL emission spectra of CuO-Fe_2O_3 Nanocomposites

UV– Visible analysis

Figure 5 displays the optical absorbance spectra of CuO-Fe_2O_3 nanocomposites, showing a maximum peak at 352 nm with significantly absorbance. Similarly, Figure 6 presents the optical absorbance spectra of CuO-Fe_2O_3 nanocomposites, also exhibiting a peak at 352 nm. The UV peaks observed in the blue region for both CuO-Mn_2O_3 and CuO-Fe_2O_3 nanocomposites confirm the nanoscale nature of the synthesized materials [9].

The optical band gap is calculated by using the relation

$$\alpha h\upsilon = A\,(h\upsilon - E_g)^n$$

where, A is a characteristic parameter independent of photon energy, h is Planck's constant, υ is the frequency of light, E_g is the optical energy band gap, and n defines the type of electronic transition. For direct allowed transitions, n = 2 and for indirect allowed transitions n=1/2. The Tauc plot method is commonly used to determine (E_g) by plotting $(\alpha h\upsilon)^2$ against hυ (photon energy). The optical band gap is estimated by identifying the linear region of the plot and extrapolating it to intersect the energy axis (x-axis) at zero. Using this method, the optical band gap was determined to be E_g=4.2 eV for CuO-Mn_2O_3 nanocomposites (Fig. 7) and E_g=3.7 eV for CuO-Fe_2O_3 nanocomposites (Fig. 8). These differences in bandgap values highlight the distinct electronic properties of the nanocomposites, crucial for optimizing their optoelectronic performance in specific applications.

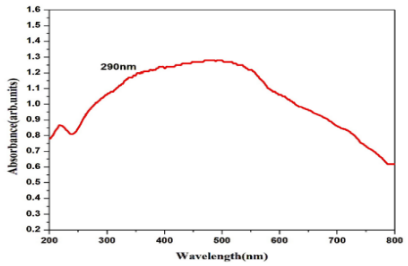

Fig. 5. Optical absorbance spectra of Mn_2O_3 nanocomposites

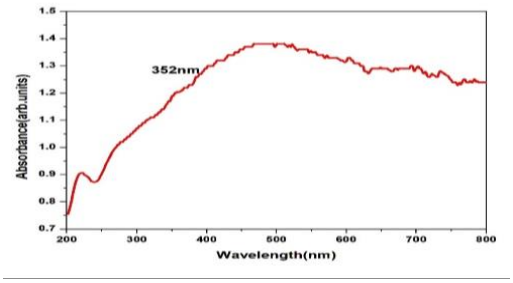

Fig. 6. Optical absorbance spectra of CuO-Fe_2O_3 nanocomposites CuO-

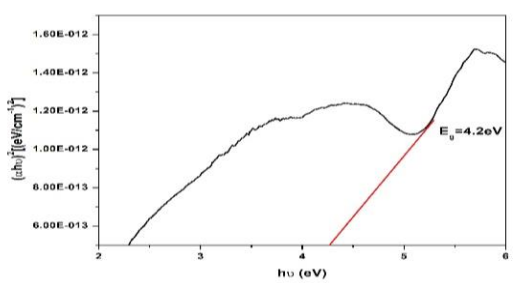

Fig. 7. Optical Energy band gap of CuO-Mn_2O_3 CuO- Nanocomposites

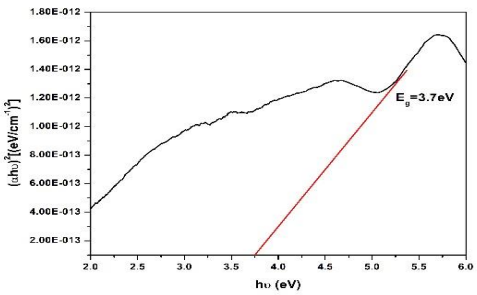

Fig. 8. Optical Energy band gap of Fe_2O_3 nanocomposites

4. Conclusion

The $CuO\text{-}Mn_2O_3$ and $CuO\text{-}Fe_2O_3$ nanocomposites synthesized by ultrasonication-assisted co-precipitation have demonstrated excellent optical and electronic properties for heavy metal sensing. UV-Vis spectroscopy confirmed strong light absorption in the visible range, while photoluminescence studies provided valuable insights into charge carrier dynamics, essential for achieving high sensor sensitivity and selectivity. The enhanced optical properties, combined with high surface area and effective electron transfer, contribute to the nanocomposites' remarkable sensitivity and low detection limits for Pb^{2+}, Cd^{2+}, and Hg^{2+} ions. These findings highlight the potential of $CuO\text{-}Mn_2O_3$ and $CuO\text{-}Fe_2O_3$ nanocomposites as efficient, cost-effective sensors for monitoring toxic metal ions in environmental applications.

References

1. Wang W., Zhou Q., Fei X., He Y., Zhang P., Zhang G., Peng L., Xie W. Synthesis of CuO Nano- and Micro-Structures and Their Raman Spectroscopic Studies. Journal of Materials Chemistry 2010; 12: DOI: 10.1039/b919043.
2. Uma B., Anantharaju K. S., Renuka L., Malini S. Synthesis of CuO Samples by Co-Precipitation and Green Mediated Combustion Routes: Comparison of Their Structural, Optical Properties, Photocatalytic, Antibacterial, Haemolytic and Cytotoxic Activities. Ceramics International, 2021.
3. Erci F., Cakir-Koc R., Yontem M., Torlak E. Synthesis of Biologically Active Copper Oxide Nanoparticles as Promising Novel Antibacterial-Antibiofilm Agents. Preparative Biochemistry & Biotechnology 2020; 50(3)**:** 238 – 248. DOI: 10.1080/10826068.2020.1723695.
4. Carraro G., Gasparotto A., Maccato C. Fe_2O_3-CuO Nanocomposites Prepared by a Two-Step Vapor Phase Strategy and Analyzed by XPS. Journal of Materials Science, 2014.
5. Wang J., Chen J., Peng L., Zhang H., Jiang Z., Xiong K., Yang Q., Chen J., Yang N. On the $CuO\text{-}Mn_2O_3$ Oxide-Pair in CuMnOx Multi-Oxide Complexes: Structural and Catalytic Studies. Journal of Catalysis 2022; 575: 151733.
6. Subban Senthil M. G. J. Manganese Oxide-Enriched Copper Oxide (Mn_2O_3/CuO) Nanocomposite Electrodes for Supercapacitor Application. Arabian Journal for Science and Engineering 2024; 49(12): DOI:10.1007/s13369-024-08860-7.
7. Bharath G., Ponpandian N. Hydroxyapatite Nanoparticles on Dendritic $\alpha\text{-}Fe_2O_3$ Hierarchical Architectures for a Heterogeneous Photocatalyst and Adsorption of Pb(II) Ions from Industrial Wastewater. RSC Advances 2015; 5: 84685 - 84693.

8. Bharathi S., Nataraj D., Mangalaraj D., Masuda Y., Sentil K., Yong K. Highly Mesoporous α-Fe_2O_3 Nanostructure Preparation, Characterization and Improved Photocatalytic Performance Towards Rhodamine B (RhB). Journal of Physics: Applied Physics 2010; 43: 015501.
9. Cavaliere-Jaricot S., Brioude A., Miele P. Ultra thin Polycrystalline Hematite and Geothite-Hematite Core-Shell Nanorods. Langmuir 2009; 25(5): 2551 - 2553.